ISBN: 978-3-95450-231-8 ISSN: 2673-5490 doi: 10.18429/JACoW-IPAC2023-TUPM095

VERIFICATION OF THE OPTICS MODEL OF THE ESR-CRYRING TRANSFER LINE AT GSI

C. Hessler †, O. Geithner, P. Schütt
GSI Helmholtzzentrum für Schwerionenforschung GmbH, Darmstadt, Germany

Abstract

Experiments at CRYRING@ESR using beams accelerated and decelerated in the accelerator chain SIS18-ESR-CRYING at GSI are considered as the first real FAIR experiments. For these experiments, CRYRING@ESR receives fast extracted beams from the ESR, which are cooled and decelerated down to about 10 MeV/u in the ESR. The beam transport from ESR to CRYRING@ESR is difficult, since part of the beamline has been reused and was not designed for such low-energy beams. Furthermore, developments inside the ESR are on-going and – especially after switching to the new FAIR control system – one could not expect that beam parameters and optics functions at the extraction point are necessarily the same as in the past. Therefore, a measurement campaign has been carried out to verify the optics model for the ESR-CRYRING@ESR beamline. The initial values for the optics functions at the ESR extraction point and the transverse emittance have also been measured. The results are discussed in this paper.

INTRODUCTION

The CRYRING@ESR [1] is a low-energy storage ring for heavy ions and it is the first accelerator realized within the scope of the FAIR project as a Swedish in-kind contribution. It can be operated with a wide range of ion species with injection energies of around 10 MeV/u and further decelerated down to a few 100 keV/u. CRYRING@ESR can be served with beam either from a local injector or from the ESR via a dedicated transfer line. The beam from ESR is fast extracted with a magnetic septum in the east long straight section near one of the main dipole magnets of the ESR. It passes then the fringe fields of this bending magnet, crosses the beamline towards cave M and approaches in close distance the beamline to cave C before it finally merges with the beamline from the local injector in the CRYRING@ESR cave (Fig. 1).

The ESR-CRYRING@ESR beamline served cave B in the past and was therefore not designed for such low-energy beams required now for CRYRING@ESR. The beamline suffers from several issues:

- Beam transport to CRYRING@ESR is often difficult and the transmission is not optimal. Beam intensity is often at the limit, which the experiment can tolerate.
- The initial values of the optics functions at the extraction point and the emittance of the extracted beam are not precisely known, neither experimentally nor theoretically, since the modelling of the beam propagation through the fringe field is difficult.
- For some dipole magnets in the beamline there was a discrepancy between the theoretical and the actually needed deflection angles, which was caused by faulty scaling of the magnet currents in the controller boards of the power converters and has been fixed in 2022.
- The beamline suffers from a cross talk with the beamline towards cave C. If the dipole magnet GTV1MU2 in the beamline towards cave C is switched off, the beam towards CRYRING@ESR changes position. The most likely reason for this behaviour is that the low rigidity beam is within reach of the magnetic field of GTV1MU2.

A better understanding of this beamline is critical for improving the beam transport and transmission. Therefore, two machine studies have been carried out in 2021 and 2022 to perform kick-response, dispersion, emittance and initial Twiss parameters measurements in order to improve the optics model of this beamline.

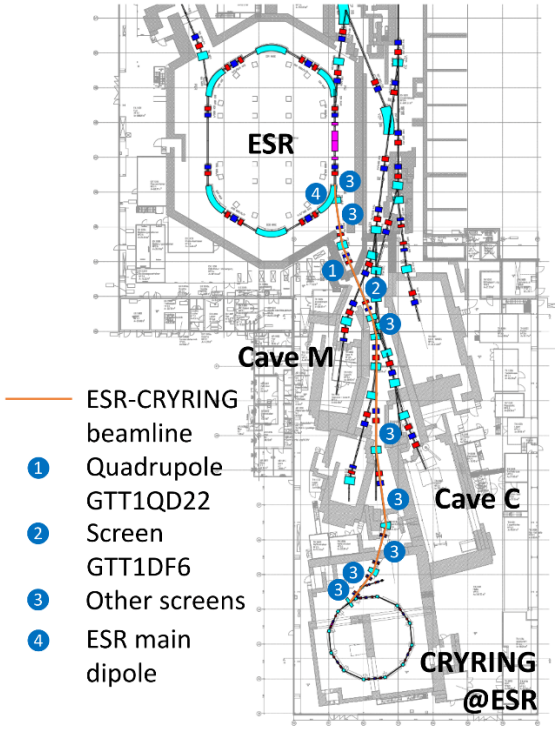

Figure 1: Location of the ESR-CRYRING beamline.

KICK-RESPONSE MEASUREMENT

Kick-response measurements have been performed during the 2021 machine study. The main motivation was to resolve the discrepancy between the theoretical and actually needed deflection angles. During this measurement different kicks α_M were applied to corrector/dipole magnets and the resulting displacements x_S on different downstream screens have been recorded. From measurement data the response matrix elements

† C.Hessler@gsi.de

ISBN: 978-3-95450-231-8 ISSN: 2673-5490 doi: 10.18429/JACoW-IPAC2023-TUPM095

$$R_{SM}^{exp} = \frac{\Delta x_S}{\Delta \alpha_M}$$

were computed and compared with response matrix elements [2]

$$R_{SM}^{theo} = \sqrt{\beta_S \beta_M}\,\sin(\mu_S - \mu_M)$$

obtained from a MAD-X [3] simulation, where β_M, β_S and μ_M, μ_S are the betatron functions and phase advances at the position of the magnet and screen, respectively. Measured and simulated response matrix elements are mostly in reasonable agreement (Fig. 2). The signs are always correct. A few matrix elements have larger discrepancies. Independently of this measurement, it has been discovered in 2022 that the controller boards of some power converters had a faulty current scaling, which was corrected before the 2022 beamtime.

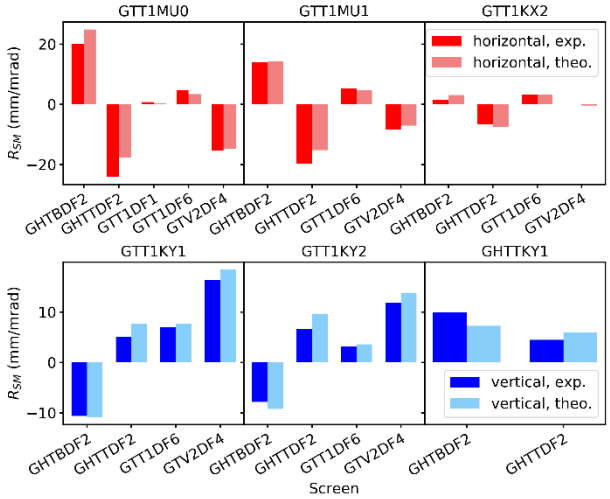

Figure 2: Comparison of selected measured (dark) and simulated (light) horizontal (red) and vertical (blue) response matrix elements.

DISPERSION MEASUREMENT

A dispersion measurement has been performed during the 2022 machine study, using a 10 MeV/u $^{197}Au^{78+}$ beam. The displacement of the beam has been recorded on all scintillating screens in the beamline as a function of momentum deviation δp. δp was changed by changing the voltage of the electron cooler and the cavity frequency in the ESR. The dispersion at each screen was obtained in the usual way by fitting a straight line to the data.

The dispersion values measured at each screen were taken as constraints in a MAD-X simulation to match the initial $D_{x,0}$ and $D_{x,0}'$ values to 5.74 m and -0.22, respectively. The dispersion curve calculated with these new start values fits well the measurement (Fig. 3). The previously used zero dispersion values have to be corrected in the model.

EMITTANCE AND TWISS PARAMETER MEASUREMENT

To measure the transverse emittance and the initial Twiss parameters a quadrupole scan and a multi-screen measurement have been performed during the machine study 2022.

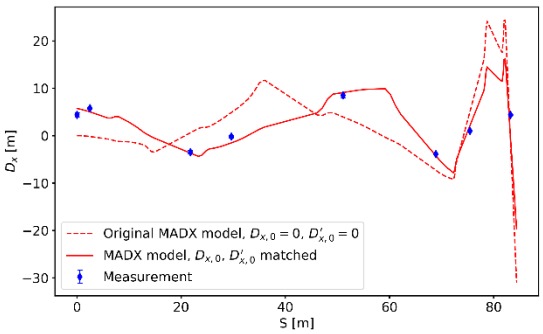

Figure 3: Measured dispersion (blue) at the different screen positions, dispersion curve matched to measurements (solid) and original model dispersion curve (dashed).

Beam Size

For this study a precise and reliable measurement of the beam size is critical. The beam images are recorded on luminescent screens with digital cameras. Different methods to compute the 1σ beam sizes from the beam profiles were investigated (Fig. 4). RMS beam sizes with 5% amplitude or 5% area cut-off [4] depend on the image section, which is used for the analysis and wrong results are produced, if the beam spot is cut on one side. Fitting a Gaussian or uniform distribution to the profiles does not well represent the data and depend on the image section. Skew Gaussian and Super Gaussian distributions proposed in [5] yield a better result, but are also not optimal. The best agreement with the data and the least sensitive to the choice of the image section is a combination of these two fit functions, a Skew Super Gaussian distribution

$$I = \frac{I_0}{\sqrt{2\pi}\sigma_0}\exp\left(\frac{-\,\mathrm{abs}(x-x_0)^n}{2\left(\sigma_0(1+\mathrm{sign}(x-x_0)E)\right)^n}\right) + I_{bg}$$

with E being the skewness and

$$\sigma = \sigma_0\left(\frac{\pi}{2}\right)^{\frac{2}{n}-1}.$$

This fit function has been used for the data analysis.

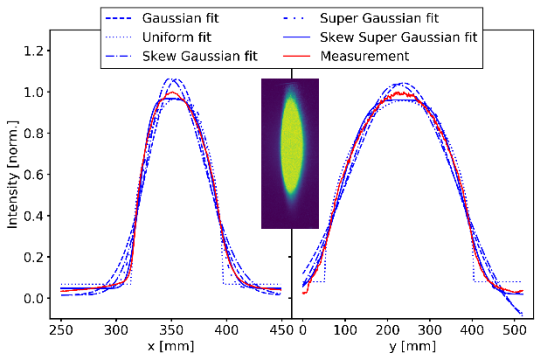

Figure 4: Comparison of different fit functions to determine the beam size.

Quadrupole Scan

The strength *KL* of quadrupole GTT1QD22 was varied in the range 0 to 1 m^{-1} and the horizontal and vertical beam sizes were measured on screen GTT1DF6. The betatron

ISBN: 978-3-95450-231-8 ISSN: 2673-5490 doi: 10.18429/JACoW-IPAC2023-TUPM095

beam size at the screen can be computed from the emittance ε and the Twiss parameters β_Q, α_Q and γ_Q in front of the quadrupole with

$$\sigma^2_{bet,S} = r^2_{11}\varepsilon\beta_Q - 2r_{11}r_{12}\varepsilon\alpha_Q + r^2_{12}\varepsilon\gamma_Q,$$

where r_{11} and r_{12} are elements of the transport matrix from the quadrupole to the screen. Usually, dispersion is neglected and using thin lens approximation the above equation becomes a parabola with the variable K [6]. A parabola fit then yields ε, β_Q and α_Q.

For the measurement described in this paper, however, the thin lens approximation criterion $(KL)^{-1} \gg L$ is not valid over a large range of KL values and the dispersion is non-zero. Therefore, the dispersion contribution has to be subtracted from the measured beam size, yielding the following system of equations:

$$\begin{pmatrix} \sigma^2_{S,1} - D^2_{S,1}\delta p^2 \\ \vdots \\ \sigma^2_{S,N} - D^2_{S,N}\delta p^2 \end{pmatrix} = \begin{pmatrix} r^2_{11,1} & 2r_{11,1}r_{12,1} & r^2_{12,1} \\ \vdots & \vdots & \vdots \\ r^2_{11,N} & 2r_{11,N}r_{12,N} & r^2_{12,N} \end{pmatrix} \cdot \begin{pmatrix} \varepsilon\beta_Q \\ -\varepsilon\alpha_Q \\ \varepsilon\gamma_Q \end{pmatrix}$$

The dispersion values and matrix elements have been obtained from MAD-X simulations for each K value using the initial $D_{x,0}$ and $D_{x,0}'$ values presented in the previous section. The system of equations has then been solved with the least squares algorithm and from the result the emittance and the Twiss parameters in front of the quadrupole have been determined using the relation $\beta\gamma\text{-}\alpha^2=1$.

To verify this analysis method, the analysis has been carried out with simulated data, which reproduced exactly the quantities used in the simulation. On the contrary, performing the usual parabola analysis with the simulated data, the obtained quantities were wrong by up to the factor 5, underlining the importance to avoid the thin-lens approximation in this case.

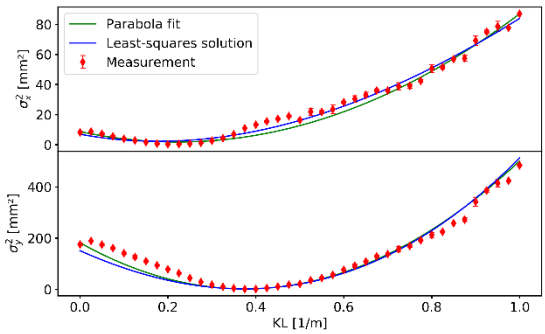

Figure 5: Squared horizontal and vertical beam sizes measured during the quadrupole scan.

Figure 5 shows the measured data, including the above-mentioned parabola and least-squares fits. Unfortunately, there were some intensity fluctuations of the ESR beam during the scan, which probably caused the fluctuations seen on the data. A MAD-X simulation was performed to match the initial Twiss parameters in the beamline to the Twiss parameters at the quadrupole obtained with the least-squares algorithm. The result is shown in Table 1.

Multi-Screen Measurement

To cross-check the quadrupole scan results, a multi-screen measurement has been performed. The beam size has been measured at all but the first and the last screens in the beamline and a least-squares analysis using the above matrix equation has been performed. In this case each line in the equation represents a measurement at a different screen and the matrix elements are of the corresponding transport matrix from the start of the beamline to the screen. From the result, the 1σ emittance and the initial Twiss parameters were directly obtained (Table 1).

Table 1: Comparison of the Results of the Two Measurement Methods with the Original Model

Parameter	Original model	Quadrupole scan	Multi-screen
$\varepsilon_{x,1\sigma}$ [µm]	1.0	0.36 ± 0.01	2.45 ± 0.04
$\beta_{x,0}$ [m]	111	150 ± 5.1	31.7 ± 0.7
$\alpha_{x,0}$ [1]	4.84	9.13 ± 0.31	2.63 ± 0.08
$\varepsilon_{y,1\sigma}$ [µm]	0.9	0.90 ± 0.01	1.32 ± 0.02
$\beta_{y,0}$ [m]	15.1	4.74 ± 1.10	4.31 ± 0.09
$\alpha_{y,0}$ [1]	3.37	1.40 ± 0.25	1.02 ± 0.03

Envelopes computed from the initial Twiss parameters measured during the quadrupole scan and multi-screen measurement are compared with the original model in Fig. 6. The curves differ from the original model. While there is a good agreement between the curves obtained by the quadrupole scan and the multi-screen measurement in the vertical plane, there is a discrepancy in the horizontal plane and some measurement points are not well represented by the model. The reason for this discrepancy is still unclear.

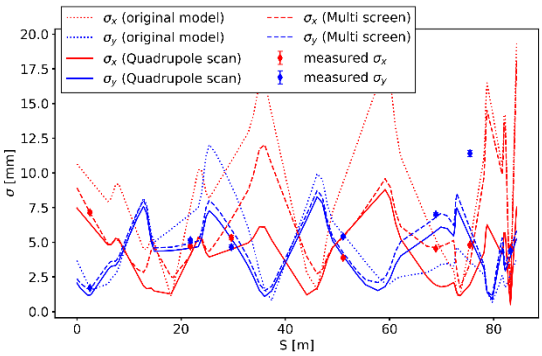

Figure 6: Comparison of beam envelopes based on the quadrupole scan and multi-screen measurement results with the original model and the measurements.

CONCLUSION AND OUTLOOK

The initial Twiss parameters, dispersion and emittance have been measured at the ESR extraction point. While the vertical emittance is in agreement with the model, other parameters of the model have to be updated. Further studies are needed to resolve discrepancies in the measurements.

ACKNOWLEDGEMENTS

The authors would like to thank M. Steck, R. Hess, C. Wetzel and R. Menges for setting up the ESR and the beamline and G. Franchetti for valuable discussions.

ISBN: 978-3-95450-231-8 ISSN: 2673-5490 doi: 10.18429/JACoW-IPAC2023-TUPM095

REFERENCES

[1] M. Lestinsky *et-al.*, "First Experiments with CRYRING@ESR", *Atoms*, vol. 10, no. 4, p. 141, Nov. 2022. doi: 10.3390/atoms10040141

[2] K. Fuchsberger, "Novel Concepts for Optimization of the CERN Large Hadron Collider Injection Lines", Ph.D. thesis, Technische Universität Wien, Wien, Austria, 2011.

[3] MAD-X, http://mad.web.cern.ch/mad/

[4] C. Limborg-Deprey *et-al.*, "Simulations for the LCLS Injector", in *Proc. FEL'07*, Novosibirsk, Russia, Aug. 2007, paper TUPPH019, pp. 260-263.

[5] F.-J. Decker, "Beam Distributions beyond RMS", SLAC report, SLAC-PUB-6684, 1994.

[6] P. Forck, "Lecture Notes on Beam Instrumentation and Diagnostics", JUAS, Archamps, 2017.